Journal of Materials Chemistry C

ROYAL SOCIETY OF CHEMISTRY

PAPER

View Article Online
View Journal | View Issue

Cite this: J. Mater. Chem. C, 2021, 9, 10975

Functionalisation of MoS_2 2D layers with diarylethene molecules†

Marc Morant-Giner, ‡ José M. Carbonell-Vilar, ‡ Marta Viciano-Chumillas, * Alicia Forment-Aliaga, * Joan Cano and Eugenio Coronado

Received 11th March 2021,
Accepted 28th July 2021

DOI: 10.1039/d1tc01133b

rsc.li/materials-c

Functionalisation of two-dimensional (2D) materials with stimuli-responsive molecules has been scarcely investigated. Here, MoS_2 layers obtained by chemical exfoliation are covalently and non-covalently functionalised using two photoswitchable diarylethene derivatives under their open- and closed-ring isomers. The choice of these light-responsive molecules is based on their excellent thermal irreversibility and fatigue resistance. The characterisation of the resultant molecular/2D heterostructures proves the successful anchoring of the molecules by both approaches as well as the influence that the driving interaction has on the photoswitching behaviour of the diarylethene isomers after their deposition on the 2D layer.

Introduction

2D materials have attracted great attention in the last few years due to the emergent properties arising from the confinement of electrons in two dimensions and to their high surface-area-to-volume ratios, which endow these materials with attractive chemical and physical properties.[1,2]

Among the 2D materials, an interesting family is that provided by layered transition metal dichalcogenides (TMDCs) with the chemical formula of MX_2 (M: transition metal, usually from groups IV–VII and X: chalcogen S, Se, or Te). Their structure consists of vertically stacked X–M–X slabs held together by weak van der Waals interactions. This structure permits easy exfoliation into ultrathin MX_2 layers by mechanical and chemical methods. TMDCs, and particularly MoS_2, have become a hot topic in materials science because of their applications in electronics,[3] optoelectronics,[4,5] sensing,[6,7] energy storage,[8] photovoltaic devices[7] and catalysis.[9,10]

The most common MoS_2 polytypes are 2H and 1T, the former being the thermodynamically stable phase with a hexagonal structural symmetry and semiconducting properties, while the latter is a metastable phase with a tetragonal structure and metallic behaviour.[11] Interestingly, molecules can tailor the MoS_2 properties by surface modification, expanding the possible applications for this 2D material.[12–15] Molecular approaches exploiting non-covalent forces *via* physisorption on MoS_2 have been developed.[12,16,17] Although these forces including electrostatic and van der Waals interactions are weak, they are effective enough to tune MoS_2 properties. Other approaches explore covalent interactions. One of them deals with coordinative functionalisation *via* coordination of S atoms of MoS_2 to metal centres using metal salts.[18] Other strategies exploit covalent functionalisation that results in the formation of S–Mo bonds at S-vacancies or C–S bonds on the basal plane.[19] While thiol derivatives are the most commonly employed molecules for the formation of S–Mo bonds,[20,21] electrophile species, such as alkyl halides and diazonium salts, have been exploited to form C–S bonds mainly due to the reactivity of the negatively charged 1T-MoS_2.[22–24] Although the 2H phase has also been modified by this approach,[25,26] click chemistry has recently become an alternative to covalently functionalise this less reactive phase under mild conditions.[27]

A step further in this research area involves introducing active molecular systems, which present bistability. Thus, smart hybrid materials can be designed to modulate the MoS_2 properties by external stimuli (light, magnetic and electric fields, *etc.*).[28,29] Among the active systems, photochromic bistable molecules undergo a reversible chemical conversion under light irradiation between two defined stable states, displaying markedly different physical or chemical properties. The fact that they have two defined states makes them excellent candidates for developing 2D light-responsive materials, where their properties are modulated by light stimuli. Some well-known examples of photochromic molecules are azobenzenes,

Instituto de Ciencia Molecular, Universitat de València, C/Catedrático José Beltrán 2, 46980 Paterna, Spain. E-mail: alicia.forment@uv.es, marta.viciano@uv.es

† Electronic supplementary information (ESI) available: Experimental section (materials; synthesis of organic molecules, composites and physical mixture; characterisation techniques; photoswitching studies methodologies). Physical and chemical characterisation of ce-MoS_2. TEM images of **MoS_2-3**. IR spectra of **2**, **3-H**, **MoS_2-2c** and **MoS_2-3c**. XPS data. Molecular representation of **3-H** (different configurations and distances). Raman and PL spectra of **2** and **3-H**. TGA analysis. Photoswitching studies of **2** and **3-H** (UV/Vis and Raman spectra) and **MoS_2-2** and **MoS_2-3** (Raman spectra). DFT and TDDFT calculation details. See DOI: 10.1039/d1tc01133b

‡ These authors contributed equally.

spiropyrans and diarylethenes.[30–32] Several researchers have focused on the use of photochromic molecules, bearing mainly azobenzene groups,[33–35] to induce optical changes into MoS_2. Nevertheless, other photochromic molecules like diarylethene derivatives remain unexplored as optical MoS_2 modulators.[36] Their photochromism arises from the reversible photoinduced cyclisation and cycloreversion reactions between the open and closed isomers, which goes with a significant change in the electronic transport through the molecules due to the rearrangement of the π-system, with on (closed isomer) and off (open isomer) states. This effect has already been proved in molecular junctions between graphene and gold electrodes.[37–39] Therefore, diarylethene derivatives could play the role of a molecular switch in the electronic connectivity of hybrid materials when diarylethenes are used as bridges between stacked or interconnected 2D layers. Moreover, this reversible photoisomerisation is accompanied by a shift of the HOMO and LUMO energy levels, which has been used to induce an optical modulation of the charge transport properties of underlying 2D materials in direct physical contact with the diarylethene molecules.[40,41] Therefore, diarylethene molecules could represent a valuable alternative as photoswitchable molecular modulators of MoS_2 flakes for optoelectronic applications. However, so far, the chemical modification of MoS_2 layers with this family of molecules remains unexplored.

In this work, we demonstrate the functionalisation of chemically exfoliated MoS_2 (ce-MoS_2) flakes with a photoswitchable diarylethene molecule *via* electrostatic and covalent approaches (Fig. 1). In the first case, a diarylethene derivative bearing two terminal amino groups is protonated (positively charged) and mixed with negatively charged 1T ce-MoS_2 flakes. In the second case, the diarylethene derivative is used to form C–S bonds with the 2D layers by a diazotisation reaction. In both cases, the symmetrically functionalised molecules may work as molecular linkers to form stacked networks of interconnected flakes. Finally, the photoswitching capacity in the solid phase of the functionalised MoS_2 materials is studied using Raman spectroscopy.

Results and discussion

Molecular functionalisation of ce-MoS_2

1T ce-MoS_2 was prepared by *n*-BuLi treatment.[8] The quality of the exfoliated material and its 1T-phase nature (Fig. S1, ESI†) were confirmed by X-ray powder diffraction (XRPD), X-ray photoelectron spectroscopy (XPS), ultraviolet/visible (UV/Vis) spectroscopy, Raman spectroscopy, transmission electron microscopy (TEM), atomic force microscopy (AFM) and thermogravimetric analysis (TGA).

Electrostatic and covalent functionalisations of ce-MoS_2 were performed using **1** in the protonated and neutral forms, respectively, with the open and closed isomers (see the Experimental section in the ESI†). **1** (and all abbreviations used for the rest of compounds without specifying o or c) denotes both isomers, *i.e.*, open (o) and closed (c) forms. The electrostatic approach was performed by mixing **1** at pH ∼ 2.8 in an EtOH/H_2O solution to afford the chloride salt, **2**, and then, the addition of MoS_2 resulted in **MoS_2-2**. Impurities were removed by three washing cycles with EtOH/H_2O (2 : 1). The covalent functionalisation approach was carried out employing diazonium derivatives. The diazonium salts were formed *in situ* by mixing **1** and sodium nitrite in a hydrochloric medium at 0 °C under an argon atmosphere.[42,43] Then, a freshly prepared aqueous suspension of ce-MoS_2 flakes was added dropwise into the reaction system, and allowed to react for 24 h at room temperature. The nucleophilic attack of the negatively charged ce-MoS_2 at the electrophilic C atom of the diazonium group leads to

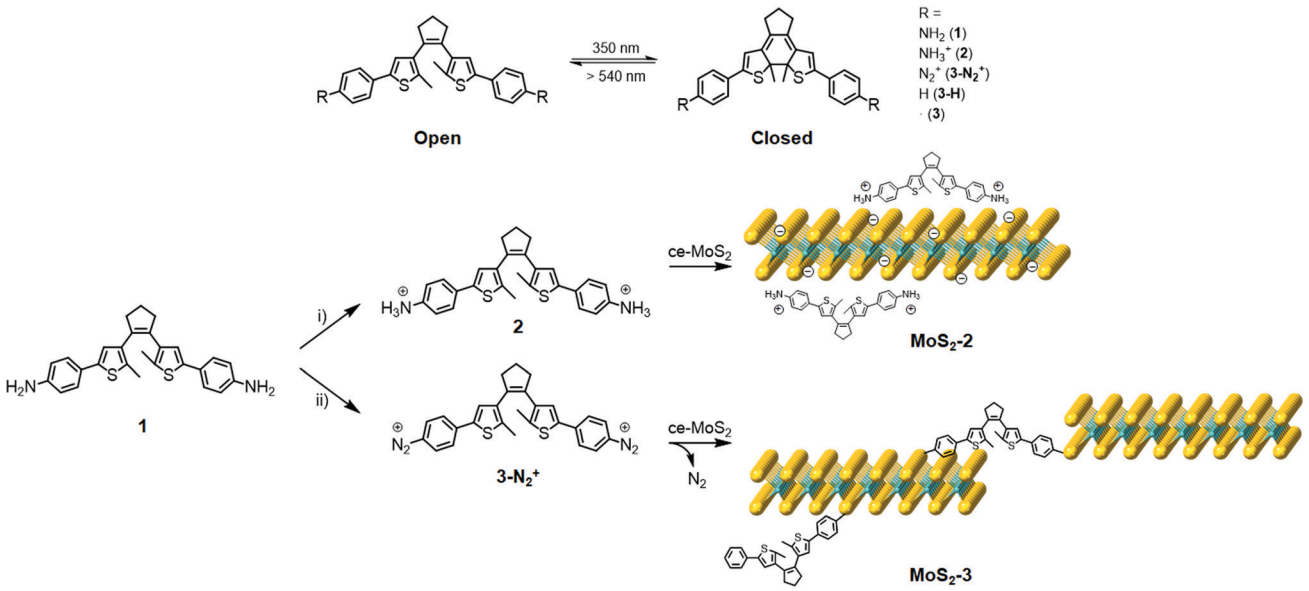

Fig. 1 Schematic representations of (top) the photoswitching behaviour of diarylethene derivatives between the open (left) and closed isomers (right), and (bottom) the electrostatic ((i) HCl in EtOH/H_2O) and covalent ((ii) $NaNO_2$; HCl) functionalisation of 1T ce-MoS_2.

the covalent functionalisation of the layers, **MoS_2-3**, with a new C–S bond. To remove physisorbed molecules, the reaction product was washed with different solvents (H_2O, DMSO and MeOH) until the absence of free diarylethene molecule in solution, which was confirmed by UV/Vis spectroscopy. For comparison purposes, a physical mixture of the open isomer of the non-substituted diarylethene molecule **3-Ho**, *i.e.*, without anchoring groups, with ce-MoS_2 was also prepared and denoted as **ce-MoS_2** + **3-Ho**.

Characterisation

The morphology of the layers after the functionalisation processes was studied by TEM (Fig. S2, ESI†), proving that the characteristic sheet-like morphology of the 2D system remains unaffected. Additionally, the TEM images show the coexistence of wrinkled and non-wrinkled MoS_2 flakes. The selected-area electron diffraction (SAED) image, taken from a non-wrinkled region, presents the typical hexagonal pattern associated with MoS_2, indicating the crystalline nature of the material. The SAED image, taken from a wrinkled region, reveals diffuse rings, which would be consistent with the presence of a polycrystalline material (*i.e.*, a collection of flakes with different orientations).

Fourier-transformed infrared (FTIR) spectroscopy was used as a first approach to confirm the MoS_2 functionalisation (Fig. 2 and Fig. S3, S4, ESI†). Although the FTIR spectra clearly prove the presence of the organic molecules on the flakes, these do not allow the exclusive vibrational modes of the open and closed rings in both composites, **MoS_2-2** and **MoS_2-3**, to be discerned. As expected, their spectra are very similar due to the resemblance of the open and closed isomers of **2** and **3-H** molecules. Interestingly, the FTIR spectra of **MoS_2-2** and **MoS_2-3** present bands between 950 and 1640 cm^{-1}, characteristic of the C=C and C–C stretching vibrations of the photoswitchable molecule.[44] Regarding **MoS_2-3** spectra, the lack of peaks associated with the aryl diazo groups[45] in the 2130 to 2315 cm^{-1} region indicates the absence of the precursor and azocoupling adducts,[46] suggesting the covalent functionalisation of MoS_2 flakes. Although the molecule contains C–S bonds in the highly substituted thiophene rings, its characteristic stretching band is reported to appear at ~800 cm^{-1}, while the presence of a band at 664 cm^{-1} in **MoS_2-3**, which is absent in **MoS_2-2**, is assigned to the C–S stretching of the resultant covalent functionalisation.[26]

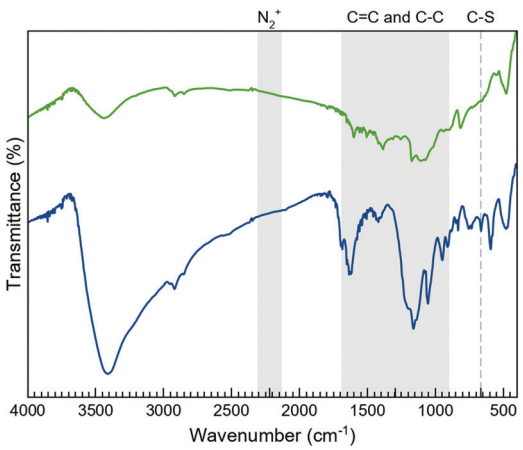

Fig. 2 FTIR spectra of **MoS_2-2o** (green) and **MoS_2-3o** (blue).

XPS spectroscopy was used to confirm the chemical composition and determine the prominent polytype in functionalised MoS_2 composites (Fig. 3). In all samples, only a small amount of oxidised material is detected, showing the stability of the 2D material after functionalisation. For the sake of clarity, Table S1 (ESI†) summarises the Mo, S, and N XPS peaks observed in **1o**, **MoS_2-2**, and **MoS_2-3**.[47–51] The XPS spectra of the open and closed isomers overlap perfectly in both **MoS_2-2** and **MoS_2-3**. However, clear differences can be found between the composites prepared by the electrostatic and covalent approaches. The Mo XPS spectra of **MoS_2-2** are dominated by Mo^{IV} (1T-MoS_2, 2H-MoS_2, and MoO_2) peaks. In the S XPS spectra, contributions from MoS_2 and the organic molecules can be clearly distinguished. Remarkably, the peaks associated with the thiophene rings have a full width at half maximum (FWHM) of ~1.1 eV, comparable to that observed in **1o**. The region of the spectra related to N shows a clear peak at ~399.4 eV, corresponding to the amino group.[52–54] The absence of Cl in the XPS survey also supports the non-covalent functionalisation between the negatively charged MoS_2 flakes and protonated amino groups. Ratios of 1T/2H MoS_2 (Mo_{1T}/Mo_{2H} = ~0.33 and 0.48 for open and closed forms, respectively) were calculated from Mo normalised areas, reflecting the coexistence of these phases in both hybrid materials in spite of an increase of the 2H phase, when compared with freshly prepared ce-MoS_2.

The XPS Mo spectra of **MoS_2-3** are dominated by Mo^{IV} (2H-MoS_2 and MoO_2) peaks. Apart from that, it is important to remark that for the S spectra, the peaks ascribed to S–C bonds are broader (with a FWHM of ~1.5 eV) than those assigned to aromatic S–C from the thiophene in **1o** (with a FWHM of ~1.1 eV). This fact confirms that new covalent bonds, as well as the thiophene rings, contribute to S–C peaks. Consistently, **MoS_2-3** does not reveal clear N signals in the N 1s region, suggesting that no nitrogen-containing by-products (like azo derivatives) or starting materials are present. Therefore, the absence of N peaks and the detection of broader S–C signals prove the efficacy of diazo moieties as leaving groups and the attachment of the diarylethene backbone to ce-MoS_2 flakes. Furthermore, the Mo XPS spectra suggest that 1T-MoS_2, obtained by the chemical exfoliation with *n*-BuLi, has been completely transformed into the most thermodynamically stable 2H-MoS_2.

The XRPD patterns of **MoS_2-2** and **MoS_2-3** resemble that of restacked ce-MoS_2 (Fig. 4). The most intense peak at ~14.3° (6.2 Å) corresponds to the (002) plane of bulk MoS_2, which indicates that some non-exfoliated MoS_2 stacks are still present after the exfoliation. However, the broadening of (002) peaks in comparison to this peak observed in the diffraction pattern of bulk MoS_2 is consistent with a drop in the periodicity along the *c*-axis, which is due to the decrease in the number of stacked layers (few-layers MoS_2). Moreover, defects from the exfoliation and functionalisation treatments can also contribute to this

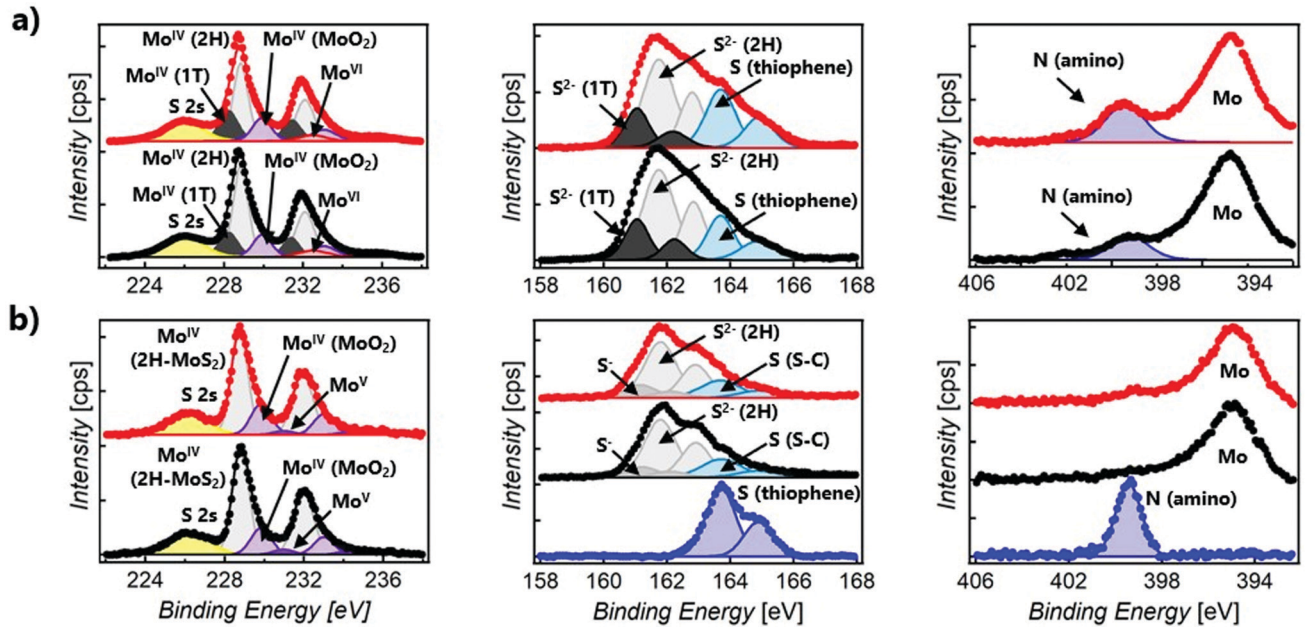

Fig. 3 Normalised Mo 3d (left), S 2p (middle) and N 1s spectra (right) of electrostatic (a) and covalent functionalised compounds (b). Each XPS spectrum is normalised with respect to the highest value registered in its envelope. Colour code: (a) **MoS_2-2o** (black) and **MoS_2-2c** (red); (b) **MoS_2-3o** (black), **MoS_2-3c** (red) and **1o** (blue).

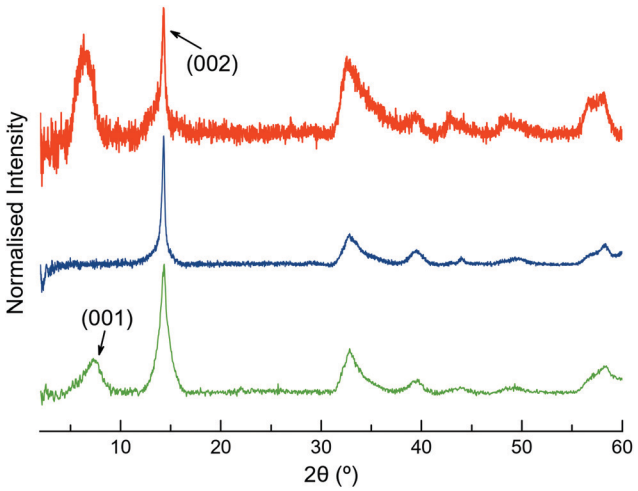

Fig. 4 Normalised XRPD patterns of restacked ce-MoS_2 flakes (green), **MoS_2-3c** (blue) and **MoS_2-2c** (orange).

broadening.[55–57] The detection of $(00l)$ peaks below $2\theta \sim 14.3^\circ$ shows that there are restacked layers with larger interlayer distances than in the bulk. In ce-MoS_2, this peak appears at $2\theta \sim 7.2^\circ$, and is commonly related to water bilayers between MoS_2 monolayers.[58,59] In the electrostatic composite, **MoS_2-2c**, such a peak is slightly shifted to $\sim 6.4^\circ$, corresponding to an interlayer spacing of 13.8 Å. This observation could be indicative of the presence of **2c** molecules forming a monolayer or bilayer, depending on the orientation adopted by the flexible molecule on the MoS_2 layer (Fig. S5, ESI†).

In contrast, no peaks below $\sim 14.3^\circ$ are observed in the covalent composite **MoS_2-3**. The presence of peaks at low 2θ values is usually ascribed to the presence of the molecule and could suggest a covalent functionalisation of the basal plane. Still, its absence in **MoS_2-3** might be related to the loss of large periodicity in the *c*-axis. Unlike Rao *et al.* who claimed layered assemblies by using a rigid linker,[23] the photochromic diarylethene molecules can either connect to different MoS_2 layers or react with just one of them due to their flexibility. Then, such pillared structures might not be formed along the whole *c*-axis, or they can present inhomogeneous interlayer distances (no periodicity). Furthermore, the absence of the peak at $2\theta \sim 7.2^\circ$, related to a bilayer of water molecules between the MoS_2 layers, can also be justified by the use of more volatile solvents during the last purification step in the synthesis of the composite.

Raman spectroscopy was performed in a second step to distinguish between the open- and closed-ring isomers of the photochromic molecule. Three different excitation wavelengths (532, 633, and 785 nm) were tested in order to find the optimum conditions.

The Raman spectra of **2** as a solid are mainly masked due to the presence of strong photoluminescence (PL), with low resolved peaks associated with the closed-ring isomer, while no peaks are detected for the open one (Fig. S6, ESI†). In **MoS_2-2**, the attachment of **2** on MoS_2 leads to the PL quenching of the organic system, probably caused by a charge transfer between the layer and the organic molecule (Fig. 5). Regarding MoS_2, the characteristic peaks of the 1T phase are clearly visible at ~ 152 (J_1) and 328 cm^{-1} (J_3). The most intense peaks detected in **MoS_2-2** spectra somehow match with those registered for **2c**, which intriguingly suggests the presence of the closed-ring isomer in both **MoS_2-2** composites. It has been previously reported that a reductive cyclisation of the open isomer can be induced in some diarylethene derivatives.[60]

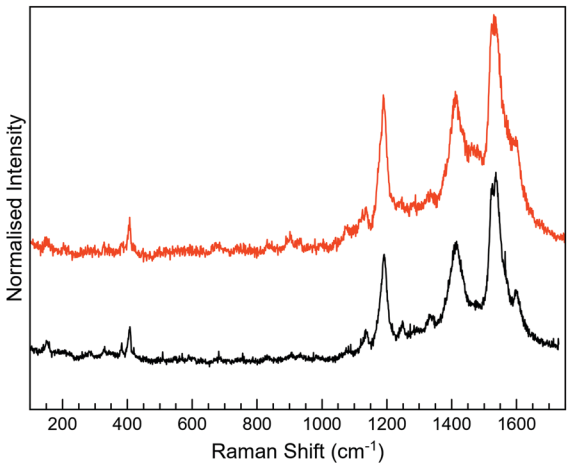

Fig. 5 Normalised Raman at a 532 nm excitation wavelength for **MoS_2-2o** (black) and **MoS_2-2c** (red).

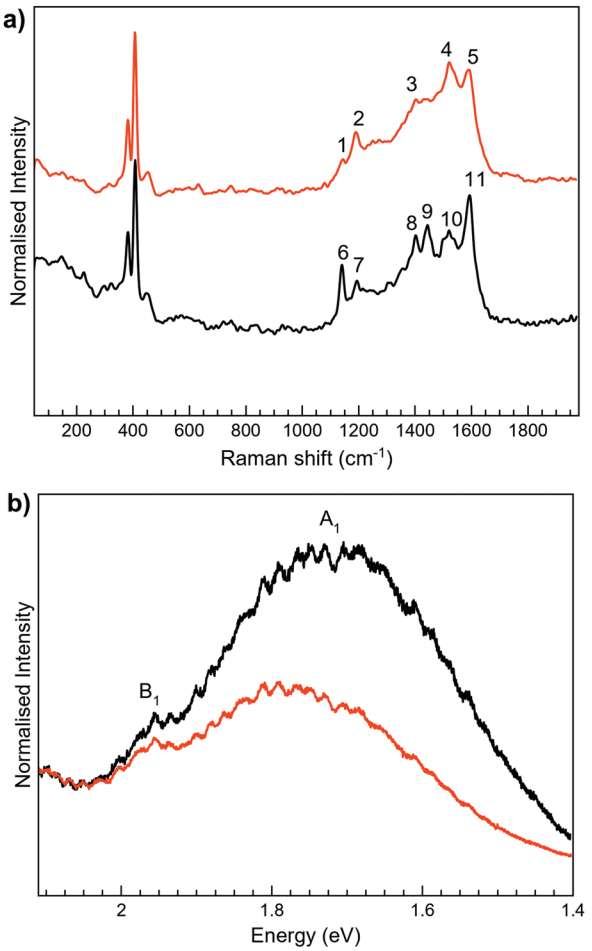

Fig. 6 Normalised Raman (a) and PL (b) spectra of **MoS_2-3o** (black) and **MoS_2-3c** (red) at 532 nm wavelength. In (a), vibration bands of **MoS_2-3c** appear at ~1141 (1), 1191 (2), 1403 (3), 1521 (4), and 1593 (5) cm^{-1} whereas for **MoS_2-3o** are at ~1141 (6), 1196 (7), 1403 (8), 1439 (9), 1520 (10), and 1597 (11) cm^{-1}.

Moreover, ce-MoS_2 can act as a reducing agent due to the accumulation of negative charge after its chemical exfoliation.[8] Thus, in this scenario, a reduction/cyclisation of **2o** becomes possible when the molecule contacts with the 2D layer, which is reflected in the Raman spectra and in the increased percentage of the 2H-MoS_2 phase.

For **3-H**, the best Raman resolution was obtained at an excitation wavelength of 785 nm (Fig. S7, ESI†). Although **3-H** exhibits PL when more energetic lasers are used (Fig. S7, ESI†), **3-H** and MoS_2 features are perfectly visible in the **MoS_2-3** composite at 532 nm (Fig. 6a), indicating, again, a PL quenching and therefore, a potential charge transfer between the organic and the inorganic components. While the peaks at ~382 and 407 cm^{-1} correspond to E^1_{2g} and A_{1g} vibrational modes of MoS_2, the peaks located in the 1100–1700 cm^{-1} range are assigned to the organic molecule,[44] which are slightly blue-shifted with respect to those arising from **MoS_2-2**. Remarkably, peaks assigned to the organic molecule in the composite are very different from those in pure **3-H** molecules (Fig. S7, ESI†). These changes can be caused by the formation of new C–S bonds due to the high electronic sensitivity of the molecule towards aromatic ring substitution[44] and additionally, to the constraints imposed by the 2D material.

The Raman peaks assigned to the organic molecule are ~1141, 1196, 1403, 1439, 1520 and 1597 cm^{-1} for **MoS_2-3o** and 1191, 1521 and 1593 cm^{-1} for **MoS_2-3c**. However, weak peaks at ~1141 and 1403 cm^{-1} attributed to **MoS_2-3o** are also visible in **MoS_2-3c**. This fact is ascribed to the synthetic procedure of the closed form of the molecule (see the ESI†), where the cyclisation reaction is stopped before reaching the entire conversion. Hence, some **MoS_2-3o** might be present as a small impurity. No *J* peaks (characteristic of 1T-MoS_2) were detected in the **MoS_2-3** spectra,[61] confirming the 2H-MoS_2 nature already determined by XPS. This fact was also supported by the presence of PL with two bands related to the A_1 and B_1 excitonic transitions at ~1.77 and 1.95 eV, characteristic of the 2H phase (Fig. 6b).

MoS_2-2, **MoS_2-3** and the organic molecule **3-H** were characterised by TGA analysis (Fig. S8, ESI†). Although the electrostatic composite **MoS_2-2** presents a larger mass loss for the open than for the closed-ring isomer, similar TGA curves were recorded for both isomers of the covalent composite, **MoS_2-3**. For all four samples, an initial weight loss lower than 5% occurs between 25 °C and 140 °C corresponding to the release of physisorbed solvent molecules. Then, in the case of **MoS_2-2**, a significantly different weight loss of ~23.1 and ~12.5% in the 140–700 °C range was found for the open and closed composites. In **MoS_2-3**, a mass drop of ~27.4% and ~21.9% in two continuous steps was detected in the 140–700 °C range for the open and closed composites, respectively. The mass loss in the 140–700 °C range arises from the removal of the organic molecules attached to the MoS_2, except for a small contribution (~3.1%) corresponding to the S degradation of MoS_2 in all samples. With these considerations, the ratios molecule : MoS_2 for **MoS_2-2o** and **MoS_2-2c** were estimated to be 0.09 and 0.04, while for **MoS_2-3,** values of 0.13 and 0.09 were estimated for the open and closed isomers, respectively. These ratios should be slightly larger due to the small amount of oxidised Mo observed by XPS that has not been considered.

In order to obtain further information, a mechanical mixture of ce-MoS_2 and **3-Ho** (**ce-MoS_2** + **3-Ho**) was prepared and measured by TGA under the same conditions. As can be seen in Fig. S8 (ESI†), the loss of the organic molecule in the mechanical mixture is sharp and takes place at almost the same temperature as the free organic molecule. However, in the **MoS_2-2** or **MoS_2-3** composite, the loss of the organic component is much more gradual and shifted to higher temperatures. These observations highlight the effective interaction between the MoS_2 layers and the diarylethene molecules, supporting the effective functionalisation of the layers, although a difference in the strength between the electrostatic and covalent interactions is not evident. Moreover, we note that the functionalisation degree of the electrostatic composite is smaller. This could be related to the efficient removal of molecules during the washing steps in the synthetic protocol. In contrast, this removal is not possible in the covalent composite since the molecules are strongly bonded. Additionally, the difference between the open and closed isomers of the electrostatic composite could point out the difficulty of the less flexible closed molecule to accommodate on the MoS_2 surface (Fig. S5, ESI†).

Photoswitching behaviour study of composites

Photoswitchable studies were performed on both isomers **MoS_2-2** and **MoS_2-3**. To gain more insight into the photoswitchable behaviour, these studies were also performed on the organic molecules, **2** and **3-H**. As observed in other protonated diarylethene derivatives,[62] **2** presents a unidirectional switching from open to closed isomers upon UV light irradiation, λ = 350 nm, that cannot be reverted upon illumination with visible light, λ = 533 nm (Fig. S9, ESI†). Regarding **3-H**, photoactive open and closed isomers are confirmed by reversible UV/Vis spectra evolution (Fig. S10, ESI†).

Although UV/Vis spectroscopy is a useful technique for colour changes, this is not the case here, since the strong absorption of MoS_2 masks the absorption bands from the organic molecules in these materials (Fig. S11, ESI†), thus preventing a clear distinction between closed and open forms. While the organic molecules are soluble systems, the prepared composites are unstable suspensions that precipitate during long-term experiments. In order to perform all experiments under equivalent conditions, the selected material was deposited onto clean SiO_2 (285 nm)/Si substrates by drop-casting their suspensions/solutions. Samples **2** and **3-H** were irradiated inside a photoreactor at 350 nm and >540 nm at different times and were studied by Raman spectroscopy (Fig. S12 and S13, ESI†). Open- to closed-ring isomer transformation was observed for **2** and **3-H** at a 350 nm irradiation wavelength, while the reverse ring-opening only occurs for **3-H** at >540 nm as expected by the photoswitching behaviour observed in the absorption spectra.

Regarding **MoS_2-2** and **MoS_2-3** composites, first attempts inside the photoreactor at the same irradiation wavelengths as the organic molecules did not affect their Raman spectra (Fig. S14 and S15, ESI†). Thus, as an alternative approach, composite samples were irradiated at different wavelengths and measured *in situ* on the same spot area with a Raman spectrophotometer at 532 nm (see the ESI† for experimental details).

Then, Raman irradiation experiments of **MoS_2-2** at all available wavelengths revealed again that both isomers behaved identically under light irradiation, *i.e.*, no significant changes in the spectra were detected, only a signal attenuation (Fig. S16, ESI†). This fact is not surprising since, as previously described, the Raman spectra of **MoS_2-2c** and **MoS_2-2o** are the same, pointing out the possibility of the presence of **2c** in both (Fig. 5). Thus, **MoS_2-2c** is a photoinactive composite as the diarylethene derivative **2c** is.

MoS_2-3 was locally irradiated and measured *in situ* with a Raman spectrometer (Fig. 7). Irradiation of **MoS_2-3o** was performed at the lowest wavelengths available in the spectrometer. The first experiments at 473 nm did not induce any change in the Raman spectra; however, after irradiation at 532 nm for

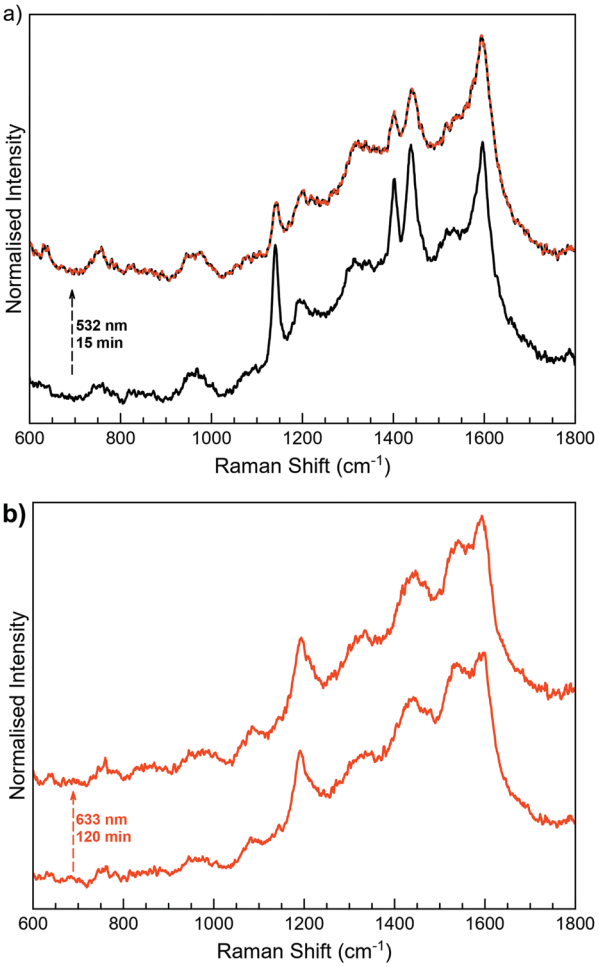

Fig. 7 Raman spectra of the irradiated **MoS_2-3o** (a) and **MoS_2-3c** (b) samples deposited on SiO_2 (285 nm)/Si substrates measured with a 532 nm excitation laser with 1% laser power. The open- and the closed-ring isomers and a mixture of both of them are represented by black, red and black-red lines, respectively. The spectra were normalised for comparison purposes.

15 minutes, the intensity of the peaks at ~1140, 1403 and 1439 cm^{-1} decreases. These results are indicative of a successful (although incomplete) open–closed photoconversion. Attempts to revert this change by irradiation at longer wavelengths (633 nm) seem to revert Raman peaks to the open form. However, this result was sample dependent, with low reproducibility, so it cannot be considered conclusive (Fig. S17, ESI†). Unidirectional switching has also been previously observed in diarylethene derivatives attached to different surfaces, and it has been blamed on the strong coupling through the covalent bonds.[37,38,63,64]

Remarkably, the observed excitation wavelengths are significantly shifted from those responsible for the photoswitching processes in the free molecule **3-H**. This difference can be due to the strong modification of the electronic structure of **3-H** once covalent C–S bonds between the diarylethene unit and the extended MoS_2 network are formed. This fact can significantly perturb the orbitals responsible for the cyclisation and cycloreversion steps, and therefore, the absorption spectrum.[65] Higher wavelengths than the ones used for the photoswitching of free diarylethene molecules have also been observed when diarylthene molecules work as coordination ligands in iridium complexes.[66,67]

Next, when **MoS_2-3c** was irradiated at 532 nm and 633 nm (Fig. 7b), no changes were observed at the 600–1800 cm^{-1} region, even after increasing the laser power or the irradiation time. The differences in the photoswitching behaviour of the directly synthesised open and closed composites **MoS_2-3** could be influenced by the different ways that open and closed diarylethene molecules can be anchored to the surface (due to different geometry and mobility) and, consequently, by a different limitation of the molecular movement in the resulting composite. By means of a molecular editor and visualizer software (Avogadro), we have studied in more detail the structure of the diarylethene derivatives used in this work. Geometrical restrictions could be significant when a diarylethene molecule is covalently bonded to the same MoS_2 flake through the two phenyl groups (low probability due to the structure of the molecule). However, these restrictions are reduced if the molecule connects two different flakes or is asymmetrically anchored by only one phenyl group. Due to the structural differences between the open and closed isomers (Fig. S5, ESI†), a double anchoring to the same MoS_2 flake is even less probable for the open form, and therefore, fewer mobility restrictions are expected for this isomer in the final composite. Remarkably, a diastereoselective cyclisation on hydrogen-bond confined diarylethene switches has already been observed, emphasising the importance of geometrical restrictions.[68]

To cast light on the experimental observations, the nature of some electronic excitations involved in the photochemical processes of **MoS_2-3** composites was theoretically studied. Models used for this purpose are detailed in the ESI† (Section S9 and Fig. S18).

In the free organic molecule, the closure and aperture of the cycle occur at 310 and 540 nm. For an electronic excitation, donor and acceptor anti-bonding and bonding molecular orbitals, respectively, make the formation of the cycle possible, and conversely, they cause its opening (Fig. 8 and Fig. S19, ESI†). When dealing with the formation of composites, the anchoring of the organic molecule to a MoS_2 layer involves creating a radical lying on the carbon atom of the molecule directly linked to the sulphur atom of the 2D layer. However, the spin density on this atom is delocalised on the layer, which transfers one electron to the attached molecule (Fig. S20, ESI†). This situation changes the electronic and photochemical properties of the lying molecules. Thus, several lower excited states appear, which are reached through electronic excitations whose ligand-to-metal charge transfer (LMCT) nature weakens the previously mentioned bonding–antibonding counterbalance responsible for the cyclisation and its opening (Fig. S21, ESI†). The presence of such states provides a path for relaxation to the starting state, inhibiting the cyclisation process, and the reverse, explaining why more energetic light sources, such as those that work on free molecules (350 and 540 nm), do not work in **MoS_2-3**. Therefore, the presence of these excited states, together with the fact that the oscillator strengths and the intensity of the absorptions are lower in **MoS_2-3**, suggest that the photoswitching process must be less efficient, as experimentally observed. Moreover, despite the main contribution of the layer in the acceptor orbital in an electronic excitation in **MoS_2-3**, the decrease of the antibonding nature between carbon atoms for the electronic excitation at 474 nm (carbon atoms which are not bonded in the donor orbital) would partially favour cyclisation, which may explain the experimental results observed under irradiation at 535 nm (Fig. S21, ESI†).

Hence, future work should be performed to avoid the hindering of the photoswitching process, probably influenced by diarylethene mobility restrictions, but mainly affected by the strong coupling with the MoS_2 layer once anchored to the surface. In this scenario, one potential strategy could deal with the use of symmetric or asymmetric diarylethene molecules

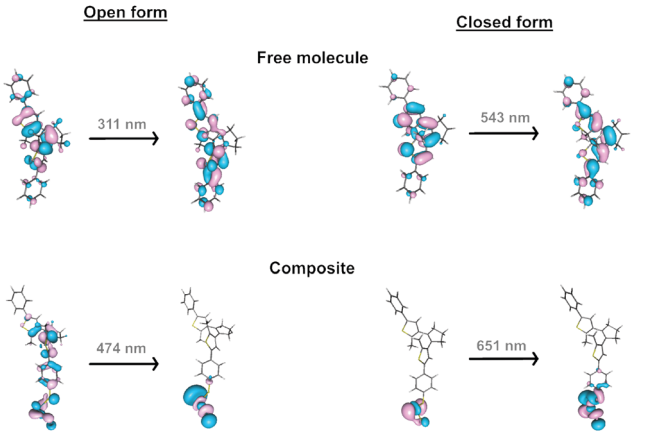

Fig. 8 Perspective views of the natural transition orbitals (NTOs) involved in some significant theoretical electronic excitations of the open and closed forms of the organic molecule and composite **MoS_2-3**. The isodensity surfaces correspond to a cut-off value of 0.05 e $bohr^{-3}$. Electrons are promoted from the orbital at the left side to the other one at the right side.

including longer substituents which would permit more flexibility and the electronic isolation of the diarylethene core from the surface.

Conclusions

This work shows for the first time MoS_2 functionalised with photoswitchable diarylethene molecules by electrostatic and covalent forces. Electrostatic functionalisation is performed by exploiting the charge interactions between the positively charged photochromic molecule and the negatively charged ce-MoS_2 flakes. Furthermore, the covalent functionalisation of ce-MoS_2 flakes is achieved by the well-known diazonium salt strategy.

By the electrostatic approach, the final composites obtained by using both, the open and the closed-ring diarylethene isomers, present identical Raman spectra and irreversible photoswitchable behaviour. Moreover, there is a charge transfer interaction between the deposited molecules and the layers, which is demonstrated by the quenching of the PL of the diarylethene derivative. Interestingly, experimental results point out a partial cyclisation of the open-ring molecule when it gets in contact with the ce-MoS_2 layers, probably due to the reducing role of the 2D layer. Consequently, ce-MoS_2 layers undergo a partial phase transition, which is unexpected for pure electrostatic interactions between the molecule and the 2D material.

Following the covalent strategy, the symmetric diarylethene molecules present two equivalent anchoring groups that can induce a cross-linking effect. However, the lack of a new periodicity observed in the *c*-axis is indicative of limited cross-linking and inhomogeneous interlayer distances. Through the covalent approach, the open and the closed-ring diarylethene isomers give rise to composites with a different Raman footprint, reflecting the stability of both isomers in contact with the MoS_2 layers. As proven by Raman spectroscopy and XPS, during the functionalisation process, 1T-MoS_2 is totally transformed into the 2H polytype, which can be due to the decrease of the negative charge accumulated on the layer when new covalent bonds are formed. Like in the electrostatic composite, the quenching of diarylethene PL denotes a charge transfer interaction between the organic and inorganic components.

Irradiation experiments reveal that the open form for the covalently functionalised MoS_2 undergoes partial close–open reactions. However, going from a closed to open material is not possible under established experimental conditions. Theoretical calculations support that the main reason behind this ineffective switching is the modification of the excited states involved in the process and the emergence of other less energetic states, which originates from the anchoring of the molecule on the MoS_2 sheet and the emergence of a radical character in the composite.

The study of these molecular/2D heterostructures may be of interest to tune the MoS_2 properties *via* the interactions established with the molecular component. Diarylethenes are envisioned as components of electronic devices due to their switchable properties induced by light, which in the present case can be attached to 2D materials to afford 2D-light-responsive hybrid systems. Therefore, further work must be done to overcome the incomplete photoconversion observed for the reported composites, which will permit the study of the photoswitching effect on the MoS_2 layer.

Conflicts of interest

There are no conflicts to declare.

Acknowledgements

The authors acknowledge the financial support from the EU (ERC-Advanced Grant MOL-2D 788222 and FET-OPEN COSMICS 766726), the Spanish MICINN (Excellence Unit María de Maeztu CEX2019-000919-M, PID2020-117152RB-I00, PID2019-109735GB-100, PID2019-104778GB-100 and EQC2018-004888-P, EQC2019-005816-P cofinanced by FEDER), and the Generalitat Valenciana (Prometeo Program of Excellence: PROMETEO/2017/066, PO FEDER Program IDIFEDER/2018/061, IDIFEDER/2020/063, AICO/2020/183). M. M.-G. thanks the Spanish MECD for the award of a FPU Grant (FPU14/04400). J. M. C.-V. thanks the Spanish MICINN for his F. P. I. Grant.

References

1 S. Z. Butler, S. M. Hollen, L. Cao, Y. Cui, J. A. Gupta, H. R. Gutiérrez, T. F. Heinz, S. S. Hong, J. Huang, A. F. Ismach, E. Johnston-Halperin, M. Kuno, V. V. Plashnitsa, R. D. Robinson, R. S. Ruoff, S. Salahuddin, J. Shan, L. Shi, M. G. Spencer, M. Terrones, W. Windl and J. E. Goldberger, *ACS Nano*, 2013, **7**, 2898–2926.
2 C. N. R. Rao, A. K. Sood, K. S. Subrahmanyam and A. Govindaraj, *Angew. Chem., Int. Ed.*, 2009, **48**, 7752–7777.
3 D. Lembke and A. Kis, *ACS Nano*, 2012, **6**, 10070–10075.
4 G. Eda and S. A. Maier, *ACS Nano*, 2013, **7**, 5660–5665.
5 H. Wang, C. Li, P. Fang, Z. Zhang and J. Z. Zhang, *Chem. Soc. Rev.*, 2018, **47**, 6101–6127.
6 M. Donarelli and L. Ottaviano, *Sensors*, 2018, **18**, 3638.
7 H. S. Nalwa, *RSC Adv.*, 2020, **10**, 30529–30602.
8 M. Morant-Giner, R. Sanchis-Gual, J. Romero, A. Alberola, L. García-Cruz, S. Agouram, M. Galbiati, N. M. Padial, J. C. Waerenborgh, C. Martí-Gastaldo, S. Tatay, A. Forment-Aliaga and E. Coronado, *Adv. Funct. Mater.*, 2018, **28**, 1706125.
9 Y. Wang, J. Mao, X. Meng, L. Yu, D. Deng and X. Bao, *Chem. Rev.*, 2019, **119**, 1806–1854.
10 R. J. Toh, Z. Sofer, J. Luxa, D. Sedmidubský and M. Pumera, *Chem. Commun.*, 2017, **53**, 3054–3057.
11 W. Zhao, J. Pan, Y. Fang, X. Che, D. Wang, K. Bu and F. Huang, *Chem. – Eur. J.*, 2018, **24**, 15942–15954.
12 A. Stergiou and N. Tagmatarchis, *Chem. – Eur. J.*, 2018, **24**, 18246–18257.
13 S. Bertolazzi, M. Gobbi, Y. Zhao, C. Backes and P. Samorì, *Chem. Soc. Rev.*, 2018, **47**, 6845–6888.

14 E. Benson, H. Zhang, S. A. Schuman, S. U. Nanayakkara, N. D. Bronstein, S. Ferrere, J. L. Blackburn and M. L. Miller, *J. Am. Chem. Soc.*, 2018, **140**(1), 441–450.
15 S. Datta, Y. Cai, I. Yudhistira, Z. Zeng, Y.-W. Zhang, H. Zhang, S. Adam, J. Wu and K. P. Loh, *Nat. Commun.*, 2017, **8**, 677.
16 L. Daukiya, J. Seibel and S. De Feyter, *Adv. Phys. X*, 2019, **4**, 1625723.
17 D. Iglesias, S. Ippolito, A. Ciesielski and P. Samorì, *Chem. Commun.*, 2020, **56**, 6878–6881.
18 S. Lei, X. Wang, B. Li, J. Kang, Y. He, A. George, L. Ge, Y. Gong, P. Dong, Z. Jin, G. Brunetto, W. Chen, Z.-T. Lin, R. Baines, D. S. Galvão, J. Lou, E. Barrera, K. Banerjee, R. Vajtai and P. Ajayan, *Nat. Nanotechnol.*, 2016, **11**, 465–471.
19 P. Vishnoi, A. Sampath, U. V. Waghmare and C. N. R. Rao, *Chem. – Eur. J.*, 2017, **23**, 886–895.
20 D. M. Sim, M. Kim, S. Yim, M.-J. Choi, J. Choi, S. Yoo and Y. S. Jung, *ACS Nano*, 2015, **9**, 12115–12123.
21 M. Makarova, Y. Okawa and M. Aono, *J. Phys. Chem. C*, 2012, **116**, 22411–22416.
22 H. Lee, S. Bak, S.-J. An, J. H. Kim, E. Yun, M. Kim, S. Seo, M. S. Jeong and H. Lee, *ACS Nano*, 2017, **11**, 12832–12839.
23 K. Pramoda, U. Gupta, I. Ahmad, R. Kumar and C. N. R. Rao, *J. Mater. Chem. A*, 2016, **4**, 8989–8994.
24 K. C. Knirsch, N. C. Berner, H. C. Nerl, C. S. Cucinotta, Z. Gholamvand, N. McEvoy, Z. Wang, I. Abramovic, P. Vecera, M. Halik, S. Sanvito, G. S. Duesberg, V. Nicolosi, F. Hauke, A. Hirsch, J. N. Coleman and C. Backes, *ACS Nano*, 2015, **9**, 6018–6030.
25 Y. Park, S. Shin, Y. An, J.-G. Ahn, G. Shin, C. Ahn, J. Bang, J. Baik, Y. Kim, J. Jung and H. Lim, *ACS Appl. Mater. Interfaces*, 2020, **12**, 40870–40878.
26 X. S. Chu, A. Yousaf, D. O. Li, A. A. Tang, A. Debnath, D. Ma, A. A. Green, E. J. G. Santos and Q. H. Wang, *Chem. Mater.*, 2018, **30**, 2112–2128.
27 M. Vera-Hidalgo, E. Giovanelli, C. Navío and E. M. Pérez, *J. Am. Chem. Soc.*, 2019, **141**, 3767–3771.
28 R. Torres-Cavanillas, M. Morant-Giner, G. Escorcia-Ariza, J. Dugay, S. Tatay, S. Cardona-Serra, M. Giménez Marqués, M. Galbiati, A. Forment-Aliaga and E. Coronado, *ChemRxiv*, 2020, DOI: 10.26434/chemrxiv.12664799.v1.
29 Y. Zhao, S. Bertolazzi, M. S. Maglione, C. Rovira, M. Mas-Torrent and P. Samorì, *Adv. Mater.*, 2020, **32**, 2000740.
30 *Molecular Switches*, ed. B. L. Feringa and W. R. Browne, Wiley-VCH Verlag GmbH & Co. KGaA, Weinheim, Germany, 2011.
31 M. Irie, *Chem. Rev.*, 2000, **100**, 1685–1716.
32 M. Irie, T. Fukaminato, K. Matsuda and S. Kobatake, *Chem. Rev.*, 2014, **114**, 12174–12277.
33 J. Li, J. Wierzbowski, Ö. Ceylan, J. Klein, F. Nisic, T. Le Anh, F. Meggendorfer, C.-A. Palma, C. Dragonetti, J. V. Barth, J. J. Finley and E. Margapoti, *Appl. Phys. Lett.*, 2014, **105**, 241116.
34 L. Cabral, F. P. Sabino, M. P. Lima, G. E. Marques, V. Lopez-Richard and J. L. F. Da Silva, *J. Phys. Chem. C*, 2018, **122**, 18895–18901.
35 Y. Zhao, S. Bertolazzi and P. Samorì, *ACS Nano*, 2019, **13**, 4814–4825.
36 S.-Z. Pu, Q. Sun, C.-B. Fan, R.-J. Wang and G. Liu, *J. Mater. Chem. C*, 2016, **4**, 3075–3093.
37 D. Dulić, S. J. van der Molen, T. Kudernac, H. T. Jonkman, J. J. D. de Jong, T. N. Bowden, J. van Esch, B. L. Feringa and B. J. van Wees, *Phys. Rev. Lett.*, 2003, **91**, 207402.
38 C. Jia, A. Migliore, N. Xin, S. Huang, J. Wang, Q. Yang, S. Wang, H. Chen, D. Wang, B. Feng, Z. Liu, G. Zhang, D.-H. Qu, H. Tian, M. A. Ratner, H. Q. Xu, A. Nitzan and X. Guo, *Science*, 2016, **352**, 1443–1445.
39 D. Kim, H. Jeong, W.-T. Hwang, Y. Jang, D. Sysoiev, E. Scheer, T. Huhn, M. Min, H. Lee and T. Lee, *Adv. Funct. Mater.*, 2015, **25**, 5918–5923.
40 H. Qiu, Z. Liu, Y. Yao, M. Herder, S. Hecht and P. Samorì, *Adv. Mater.*, 2020, **32**, 1907903.
41 H. Qiu, Y. Zhao, Z. Liu, M. Herder, S. Hecht and P. Samorì, *Adv. Mater.*, 2019, **31**, 1903402.
42 S. Baranton and D. Belanger, *J. Phys. Chem. B*, 2005, **109**, 24401–24410.
43 D. Hetemi, V. Noël and J. Pinson, *Biosensors*, 2020, **10**, 4.
44 J. J. D. de Jong, W. R. Browne, M. Walko, L. N. Lucas, L. J. Barrett, J. J. McGarvey, J. H. van Esch and B. L. Feringa, *Org. Biomol. Chem.*, 2006, **4**, 2387–2392.
45 K. Nakamoto, *Infrared and Raman Spectra of Inorganic and Coordination Compounds*, John Wiley & Sons Inc., New York, 4th edn, 1997.
46 S. Mahouche-Chergui, S. Gam-Derouich, C. Mangeney and M. M. Chehimi, *Chem. Soc. Rev.*, 2011, **40**, 4143–4166.
47 O. L. Li, Z. Shi, H. Lee and T. Ishizaki, *Sci. Rep.*, 2019, **9**, 12704.
48 J. Baltrusaitis, P. M. Jayaweera and V. H. Grassian, *Phys. Chem. Chem. Phys.*, 2009, **11**, 8295.
49 Y. Sun, X. Hu, W. Luo and Y. Huang, *J. Mater. Chem.*, 2012, **22**, 425–431.
50 J.-G. Choi and L. T. Thompson, *Appl. Surf. Sci.*, 1996, **93**, 143–149.
51 X. Geng, W. Sun, W. Wu, B. Chen, A. Al-Hilo, M. Benamara, H. Zhu, F. Watanabe, J. Cui and T. Chen, *Nat. Commun.*, 2016, **7**, 10672.
52 Q. Liu, X. Li, Q. He, A. Khalil, D. Liu, T. Xiang, X. Wu and L. Song, *Small*, 2015, **11**, 5556–5564.
53 F. Z. Wang, M. J. Zheng, B. Zhang, C. Q. Zhu, Q. Li, L. Ma and W. Z. Shen, *Sci. Rep.*, 2016, **6**, 31092.
54 M. Kehrer, J. Duchoslav, A. Hinterreiter, M. Cobet, A. Mehic, T. Stehrer and D. Stifter, *Plasma Process. Polym.*, 2019, **16**, 1800160.
55 H. Jensen, J. H. Pedersen, J. E. JØrgensen, J. S. Pedersen, K. D. Joensen, S. B. Iversen and E. G. SØgaard, *J. Exp. Nanosci.*, 2006, **1**, 355–373.
56 G. Du, Z. Guo, S. Wang, R. Zeng, Z. Chen and H. Liu, *Chem. Commun.*, 2010, **46**, 1106–1108.
57 T. Ungár, *Scr. Mater.*, 2004, **51**, 777–781.
58 P. Joensen, E. D. Crozier, N. Alberding and R. F. Frindt, *J. Phys. C: Solid State Phys.*, 1987, **20**, 4043.
59 M. Acerce, D. Voiry and M. Chhowalla, *Nat. Nanotechnol.*, 2015, **10**, 313–318.

60 B. Gorodetsky, H. D. Samachetty, R. L. Donkers, M. S. Workentin and N. R. Branda, *Angew. Chem., Int. Ed.*, 2004, **43**, 2812–2815.
61 N. H. Attanayake, A. C. Thenuwara, A. Patra, Y. V. Aulin, T. M. Tran, H. Chakraborty, E. Borguet, M. L. Klein, J. P. Perdew and D. R. Strongin, *ACS Energy Lett.*, 2018, **3**, 7–13.
62 H. Liu, X. Zhang, Z. Gao and Y. Chen, *J. Phys. Chem. A*, 2012, **116**, 9900–9903.
63 A. C. Whalley, M. L. Steigerwald, X. Guo and C. Nuckolls, *J. Am. Chem. Soc.*, 2007, **129**, 12590–12591.
64 C. Jia, J. Wang, C. Yao, Y. Cao, Y. Zhong, Z. Liu, Z. Liu and X. Guo, *Angew. Chem., Int. Ed.*, 2013, **52**, 8666–8670.
65 A. Staykov, J. Areephong, W. R. Browne, B. L. Feringa and K. Yoshizawa, *ACS Nano*, 2011, **5**, 1165–1178.
66 W. Tan, Q. Zhang, J. Zhang and H. Tian, *Org. Lett.*, 2009, **11**, 161–164.
67 W. Tan, J. Zhou, F. Li, T. Yi and H. Tian, *Chem. – An Asian J.*, 2011, **6**, 1263–1268.
68 K. Uchida, M. Walko, J. J. D. de Jong, S. Sukata, S. Kobatake, A. Meetsma, J. van Esch and B. L. Feringa, *Org. Biomol. Chem.*, 2006, **4**, 1002.